LIQUIDUS PHASES OF THE RICHARDTON H5 CHONDRITE AT HIGH PRESSURES AND TEMPERATURES.

M. Channon[1], J. Garber[2], L. R. Danielson[3] and K. Righter[3], [1]School of Earth and Space Exploration, Arizona State University, Box 871404 Tempe, AZ, 85287 (melanie.channon@asu.edu), [2]College of Geology, The University of Texas at Austin, 1 University Station C1100, Austin, TX 78712, [3]NASA, Johnson Space Center, 2101 NASA Road 1, Houston, TX 77058.

Introduction: Part of early mantle evolution may include a magma ocean, where core formation began before the proto-Earth reached half of its present radius [1]. Temperatures were high and bombardment and accretion were still occurring, suggesting that the proto-Earth consisted of a core and an at least partially liquid mantle, the magma ocean. As the Earth accreted, pressure near the core increased and the magma ocean decreased in volume and became shallower as it began to cool and solidify. As crystals settled, or floated, the composition of the magma ocean could change significantly and begin to crystallize different minerals from the residual liquid. Therefore, the mantle may be stratified following the P-T phase diagram for the bulk silicate Earth. To understand mantle evolution, it is necessary to know liquidus phase relations at high pressures and temperatures. In order to model the evolution of the magma ocean, high pressure and temperature experiments have been conducted to simulate the crystallization process using a range of materials that most likely resemble the bulk composition of the early Earth.

A single representative bulk Earth material may not exist [2], which makes it important to study a variety of materials. Allende [1], a carbonaceous chondrite, peridotite [3], the composition of the upper mantle, and Richardton [4,5], an ordinary H5 chondrite have been previously used as starting materials. Richardton, however; has not yet been fully explored; therefore this project uses Richardton as the starting material, and concentrates on the liquidus phases and location.

Experimental Methods: The experiments were performed on the 800 ton multi-anvil press in the High Pressure Laboratory at NASA Johnson Space Center. A 10/5 assembly developed by Diedrich and Leinenweber was used in all runs. The assembly was held in a 10 mm edge length injection-molded spinel octahedron, and WC cubes with 5 mm edge length truncations. The temperature was measured using WRe5/WRe26 thermocouples. Experiments were conducted by increasing the pressure over a duration of 6-48 hours. After target pressure was reached, the runs were slowly heated and left at target temperature for a duration of 5-55 minutes. This was followed by immediate quench by turning off the power source.

The calibrations were done by comparing press load to pressures of known phase transitions. The starting material used was forsterite, and was pressurized to find the olivine-wadsleyite (ol-wad) and wadsleyite-ringwooding (wad-ring) transition phases.

The octahedra were recovered and mounted in epoxy resin. The assembly was then cut to the diamond capsule using a diamond blade and remounted in epoxy resin. The diamond capsule was ground with 15 micron diamond polish to reveal the sample inside, which was further polished for analysis.

Analytical Techniques: The Cameca SX100 at NASA JSC was used to determine composition of silicates and metals. The beam conditions were 20kV accelerating voltage and 20μA sample current. Liquids in the sample do not quench to a homogeneous glass, so the average liquid composition was obtained by an average of up to 30 point line analyses ~500μm long.

Raman spectroscopy was used to determine the mineral structure. Raman scattering measurements were made using a Jobin-Yvon Triax 550 spectrograph and a LabRAM HR High Resolution Raman Microscope. Scattering was excited by the 514.33nm line of a coherent Ar+ laser. The scattered radiation was collected through a long-working distance 50 x objective.

Results: Eleven successful runs were achieved and are summarized in Table 1. These data were added to previous runs in a P-T phase diagram in Figure 1. The portion of the liquidus line contributed by this project only spans one liquidus phase, majorite garnet. The olivine-garnet (ol-gt) cotectic in the Richardton phase diagram exists at a lower temperature and higher pressure than in the peridotite phase diagram [3]. The ol-gt cotectic is also at a higher pressure than in the Allende phase diagram [1], but at the same temperature. The majorite liquidus is significantly steeper than both the peridotite and Allende P-T diagrams, over 1.5 times steeper than peridotite, and over 5 times steeper than Allende. The ol-wad transition in Richardton happens at a higher pressure than peridotite and Allende. The wad-ring transition in Richardton happens at a slightly higher pressure than the peridotite transition, but a much higher pressure than the Allende transition.

The liquidus temperatures in multi-phase runs were determined with the thermal model of [6]. The distance from the hotspot to the liquidus (Figure 2) was combined with the temperature gradient data in order to calculate the temperature at the liquidus boundary.

The K_D's, the element ratio in the solid over the element ratio in the liquid, calculated for various ele-

ment ratios in the majorite garnet found in the experiments are: $K_D(Fe/Mg) = 0.5$, $K_D(Ca/Al) = 0.1$, $K_D(Si/Mg) = 1.1$, $K_D(Al/Si) = 5.0$.

Table 1. List of experiments. Abbreviations are maj – majorite garnet, ol – olivine, liq – liquid, cpx – high Ca pyroxene, opx – low Ca pyroxene, wad – wadsleyite.

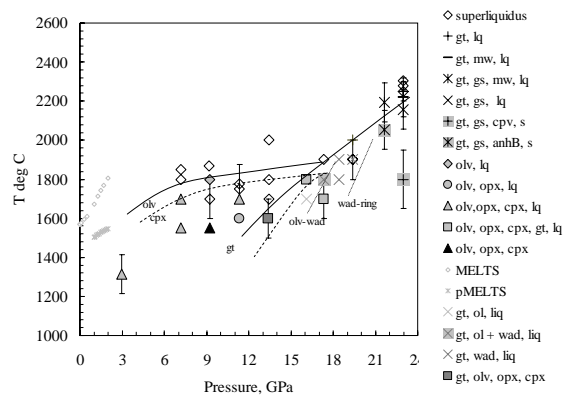| Run #	P (GPa)	Temp. (°C)	Time (min)	Phases Identified
33	16.1	1700±18	50	maj, ol, liq
34	13.4	1600±20	55	maj, ol, cpx, opx
35	18.4	1800±18	30	maj, wad, liq
38	17.3	1700±20	52	maj, ol, cpx, opx, liq
39	17.3	1800±18	30	maj, ol + wad, liq
41	16.1	1800±18	31	maj, ol, cpx, opx, liq
42	17.3	1900±18	15	superliquidus
43	18.4	1900±18	10	maj, wad, liq
44	19.4	2000±18	7	maj, liq
45	19.4	1900±18	15	maj, wad, liq
47	19.4	1900±20	14	superliquidus

Figure 1. Phase diagram of the Richardton H5 chondrite using previous data from [5] and data from this study.

Discussion: The experiments in this project were held at target temperature longer than [3] below 2000°C, and similar to their run time at 2000°C. Experiments were held at similar times to [1] below 1900°C, and slightly longer above that. It is concluded that these run times allowed equilibrium to be approached because there was no chemical zoning of solid phases. More evidence for approaching equilibrium is suggested by the $K_D^{(Fe/Mg)}$ of olivine in our experiments that have been relatively constant at 0.6 [7].

The K_D's above were used to predict the composition of the residual melt of the magma ocean after garnet is crystallized. Simply crystallizing garnet out of the Richardton material would not produce a peri-

dotite-like composition in the residual material. Using the Richardton elemental ratio compositions as a starting point then removing majorite garnet, it was found that Si/Mg is a close match at 40% removal, but, Al/Si is too high, and both Fe/Mg and Ca/Al are much too low. However, prior crystallization of lower mantle phases such as Mg-perovskite, $(Mg, Fe)SiO_3$, may change the K_D values for garnet, giving a different residual material possibly similar to peridotite. Thus, Richardton may not be ruled out as a bulk Earth material analog.
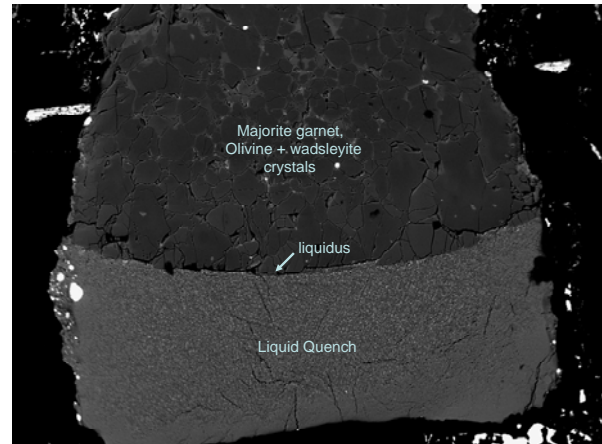

Figure 2. BSE image of run 39. The FOV is 1.5mm. The hotspot in this sample was at the bottom of the liquid quench phase.

Conclusions: In general, many of the phase transitions (e.g. the ol-gt cotectic and the ol-wad-ring transitions) occur at a higher pressure in Richardton than in Allende and peridotite. The high pressure garnet cotectic for Richardton was not found, but this trend suggests that it too would occur at a greater pressure and temperature than Allende and peridotite. If the magma ocean was like Richardton in composition, these results would favor a magma ocean model that was hot (up to 3000°C at the bottom) and deep (up to 3000 km).

References: [1] Agee C. B. et al. (1995) *JGR, 100,* 17,725–17,740. [2] Drake M. J. and Righter K. (2002) *Nature*, 416, 39-44. [3] Zhang J. and Herzberg C. (1994) *JGR, 99*, 17, 729-17, 742. [4] Mason, B. (1979) *Data of Geochemistry* (ed. Fleischer, M., US Dept of the Interior, Geological Survey Washington D.C.). [5] Danielson L. R. et al. (2004) *Eos Trans. AGU*, 85(47), Fall Meet. Suppl., V43C-1432. [6] Hernlund J. W. et al. (2000) *Eos Trans. AGU*, 81(48) [7] Gaetani G. A. and Grove T. L. (1998) *Contrib Mineral Petrol*, 131, 323-346.